Diffusiophoresis in Multivalent Electrolytes

Jessica L. Wilson, Suin Shim, Yingxian Estella Yu, Ankur Gupta, and Howard A.

Stone*

Department of Mechanical and Aerospace Engineering, Princeton University, Princeton,

NJ 08544

E-mail: hastone@princeton.edu

Abstract

Diffusiophoresis is the spontaneous movement of colloidal particles in a concentration gradient of solutes. As a small-scale phenomenon that harnesses energy from concentration gradients, diffusiophoresis may prove useful for passively manipulating particles in lab-on-a-chip type applications as well as configurations involving interfaces. Though naturally occurring ions are often multivalent, experimental studies on diffusiophoresis have been mostly limited to monovalent electrolytes. In this work, we investigate the motion of negatively charged polystyrene particles in one-dimensional salt gradients for a variety of multivalent electrolytes. We develop a one-dimensional model and obtain good agreement between our experimental and modeling results with no fitting parameters. Our results indicate that the ambipolar diffusivity, which is dependent on the valence combination of cations and anions, dictates the diffusiophoretic motion of the particles by controlling the timescale at which the electrolyte concentration evolves. In addition, the ion valences also modify the electrophoretic and chemiphoretic contributions to the diffusiophoretic mobility of the particles. Our results are applicable to systems where the chemical concentration gradient is comprised of multivalent ions, and motivate future research to manipulate particles by exploiting ion valence.

Keywords: transport phenomena, valence, electrolytes, diffusiophoresis

Introduction

Diffusiophoresis, first described by Derjaguin et al. 1 over seven decades ago, refers to particle motions driven by chemical gradients. Typically, a gradient of cations and anions with a difference of respective diffusivities (D_+ and D_-) produces a local electric field that sets charged particles into motion; this response is equivalent to electrophoresis. Simultaneously, the presence of a chemical gradient produces local osmotic pressure variations at the scale of a particle, which also produces particle movement; this is the chemiphoretic contribution to motion. $^{2-4}$ The two chemical contributions, electrophoresis and chemiphoresis, account for diffusiophoretic motions. The corresponding flows driven by chemical gradients tangent to a stationary surface are referred to as diffusio-osmosis. Nearly all experimental studies $^{5-12}$ have considered the case of electrolytes with equal valence for the cations and anions ($z_+ = z_-$ as for NaCl, KCl, etc.). Here we present experimental results of diffusiophoretic particle motion in non-z: z electrolytes and compare the measurements with the recent theoretical predictions of Gupta et al. 13

During the past decade there have been a wide range of experimental, numerical and theoretical studies of diffusiophoretic transport. For example, researchers have demonstrated focusing and spreading of particle streams, 7,14 particle extraction from (or delivery to) deadend pores, 8,15 the formation, temperature triggering and combination of solutal beacons for directing particle motion, 9,10 particle accumulation by competing pressure-driven flow and diffusiophoresis, $^{15-17}$ long-lived transient effects, 11 diffusiophoretic motion of particles in surfactant gradients and the role of diffusiophoresis in laundry detergency, 12,18 dissolved CO_2 as a driver of diffusiophoresis for manipulating particles in flows, 19 among others. $^{20-27}$

Of course, early work in the field identified many of these ideas including approaches

to particle separations⁵ and surface coating. 6,28,29 In some cases, there are detailed comparisons of experiment and theory, though the work we are aware of focuses on 1:1 electrolytes. Although recent work has started to explore multivalent effects, 30 no literature has yet systematically investigated non-z:z electrolytes experimentally or compared results with theoretical predictions. Solutions of non-z: z electrolytes are expected to produce differences in diffusiophoretic motions as a consequence of (i) changes in the ambipolar diffusivity (see Equation (4)) that characterizes the effective diffusivity of a salt, and (ii) changes to both the electrophoretic and chemiphoretic contributions to the diffusiophoretic velocity for a given concentration of electrolyte. 13

In this article, we tackle this question of the effect of non-z:z electrolytes on particle movement using experiments in a microfluidic device with dead-end pores, where a chemical concentration difference between the main channel and the dead-end pores is responsible for particle motion. In the first section we describe the experimental approach which includes two types of experiments, an entrainment experiment and a novel "compaction" experiment. The second section includes a summary of our mathematical model of diffusiophoretic transport for non-z:z electrolytes and a comparison of experiments and the model, including experiments with $(z_+:z_-)$ a 1:1 electrolyte (NaCl), two 2:2 electrolytes (MgSO₄, CaSO₄), a 1:2 electrolyte (Na₂SO₄) and two 2:1 (MgCl₂, CaCl₂) electrolytes. In the third section, we discuss the comparison of the experiments and the model, use a similarity solution to understand the observed trends, and discuss the significance of the ambipolar diffusivity on the diffusiophoretic motion of the particles. The last section provides a brief summary and conclusions.

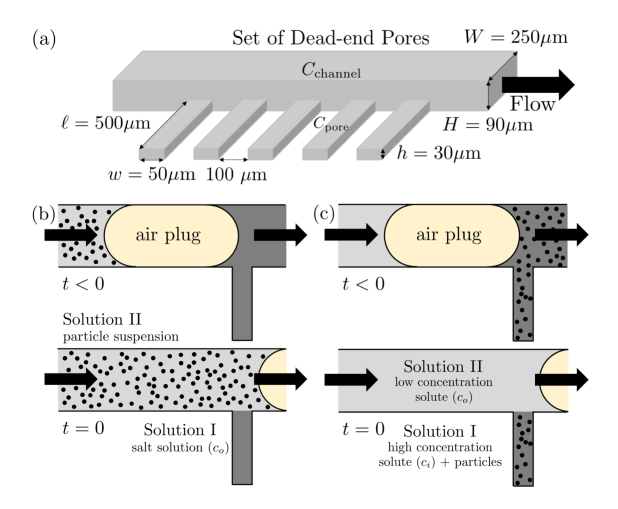


Figure 1: (a) Schematic showing the dimensions of the dead-end pores. We conducted two different types of experiments with the dead-end pores. (b) In the entrainment experiments Solution II contains particles (in DI water), which become entrained in the pore, initially filled with Solution I, due to the concentration gradient. (c) In the compaction experiments, pores are initially filled with a particle suspension (Solution I). Here, Solution II does not contain particles, but creates a concentration gradient of salt.

Materials and Methods

PDMS Microfluidic Channel

The PDMS channels are prepared using standard soft lithography procedures where the elastomer base and silicone elastomer curing agent (Dow Corning, Sylgard 184) were mixed at a ratio of 10:1. The channel design and dimensions are shown in Fig. 1. The width and height of the main channel are 250 μ m and 90 μ m respectively. The width and the height of the dead-end pores are 50 μ m and 30 μ m respectively. The length of the dead-end pores is 500 μ m, and the spacing between them is 100 μ m.

Salt Solutions

For salts we used Na₂SO₄ (Fisher Chemical, Lot 931634), CaCl₂·2H₂O, MgSO₄, MgCl₂, and NaCl (Sigma Aldrich; Lot SLBR6503V, Lot 095K0117, Lot SLBT5102, and Lot SLBB9515V, respectively) and CaSO₄ (Drierite, Lot 13001). Soluble salts were directly dissolved in DI

water (Milli-Q, EMD Millipore) to make 100 mM solutions, then the solutions were further diluted for experiments. $CaSO_4$ has poor solubility, so the solution was created by submerging Drierite pellets in DI H_2O . After the slurry settled we were left with a saturated (approximately 20 mM) solution ($CaSO_4$ has a solubility of 0.27 g/100 mL at 20 °C),³¹ a portion of which we later combined with an equal volume of DI water at 22 °C for an approximately 10 mM solution. Portions of this solution were further diluted.

Table 1: Table of experimental concentrations for all salts studied, NaCl, Na₂SO₄, CaCl₂, CaSO₄, MgCl₂, and MgSO₄.

Experiment Type	Solution I	Solution II
Entrainment	10 mM	DI H ₂ O + particles
Compaction	1 mM + particles	0.1 mM

Particle Suspensions

We used 1 μ m diameter fluorescent (540/560) polystyrene latex FluoSpheres particle (Molecular Probes). The particles were dispersed in a salt solution of interest at the volume fraction of 2.62×10^{-4} .

Experimental Protocol

The fluorescent images were recorded every second for 300 seconds using an inverted microscope (Leica, DMI4000B). In order to prevent evaporation-induced dry air plugs in the pores, which lead to poor connection between two solutions, most data were collected at or above a relative humidity (RH) of 20 %.

Entrainment Experiments

Every experiment uses two aqueous solutions, called Solution I (10 mM) and Solution II (particles in DI water – no electrolytes). In an initially empty channel, Solution I is injected manually. Once it has filled the main channel, we block the outlet and apply gentle pressure

to manually fill the pores. After the pores are filled with Solution I, the plug blocking the outlet is removed and the syringe containing Solution II is connected to the channel inlet. In order to introduce an air plug between two solutions, 2-4 mm of the tip of the connecting tubing is left empty. Initially separated from Solution I by an air plug, Solution II is flown into the channel at 90 μ L/hr. After the two solutions come into contact at the pore entrance, the rate of injection of Solution II is reduced to 30 μ L/hr.

Compaction Experiments

In an initially empty channel, Solution I (particles in a 1 mM solution) is injected at a flow rate 90 μ L/hr using a syringe pump (Harvard Apparatus). Once the main channel is filled, we block the outlet and reduce the flow rate to 30 μ L/hr. Due to increased pressure in the entire channel, the pores gradually fill with Solution I. As a result, we obtain particles that are uniformly distributed in the pores as an initial condition. After the pores are filled with Solution I, the plug blocking the outlet is removed and the syringe containing Solution II (0.1 mM) is connected to the channel inlet. Separated from Solution I by an air plug, Solution II is injected at 90 μ L/hr, then slowed to 30 μ L/hr after the two solutions come into contact at the pore entrance. We used lower concentrations (see Table 1) for the compaction experiments because the particles formed clumps and stuck to walls when placed in 10 mM solutions of electrolytes with +2 counterions. In this case, we may have exceeded the Critical Coagulation Concentration(CCC), which is strongly dependent on the valence of counterions.

Results

Experimental Data from Entrainment and Compaction Experiments

In order to study the effect of valence on the diffusiophoresis of particles, we use a dead-end pore geometry (Fig. 1). The channel has both a main channel and small pores connected to the side wall of the main channel. After filling the pores with an aqueous solution,

another aqueous solution is flown through the main channel to generate a one-dimensional concentration gradient. The salts used for the experiments were NaCl, Na₂SO₄, CaCl₂, CaSO₄, MgCl₂, and MgSO₄. Two types of experiment were conducted. In the entrainment experiments (Fig. 1(b)), the pores are initially filled with a salt solution (10 mM) without particles. As we introduce the second solution (particle suspension in DI water with particle volume fraction $\approx 2.6 \times 10^{-4}$) after an air plug (for details, see experimental protocol), the particles move into the pores starting at time t=0. The entrainment experiments are typical of recent research in diffusiophoresis.^{8,15} In the compaction experiments (Fig. 1(c)), the pores are initially filled with particles suspended in a high concentration salt solution (1 mM), and a low concentration salt solution (0.1 mM) is introduced in the main channel (t=0). For all choices of electrolyte, the diffusiophoretic motion generated moves particles further into a pore; for the compaction experiments, the total particle number is conserved. Images of representative entrainment and compaction experiments are shown in Fig. 2(a-c: entrainment; e-g: compaction). For both types of experiments we measure the fluorescence intensity of the particles, which is a proxy for particle concentration, along the length of the pores and plot the gray value (Fig. 2(d, h)). Note that the concentrations of salts used in the two configurations are different from each other.

There are advantages and disadvantages to the two experimental configurations. Since the data for the entrainment experiment (Fig. 2(d)) shows a clear maximum at every time point, it enables a more accurate prediction of the diffusiophoretic velocity as compared to the compaction experiments where multiple peaks are obtained in the intensity data (Fig. 2(h)). However, in the entrainment experiments, since the number of particles in the pores increases with time, the theoretical model is singular at the mouth of the pore (see Materials and Methods). In contrast, for compaction experiments, the area under the curve is constant, indicative of a fixed number of particles (Fig. 2(h), and Supporting Information), and the theoretical model does not have a singularity.

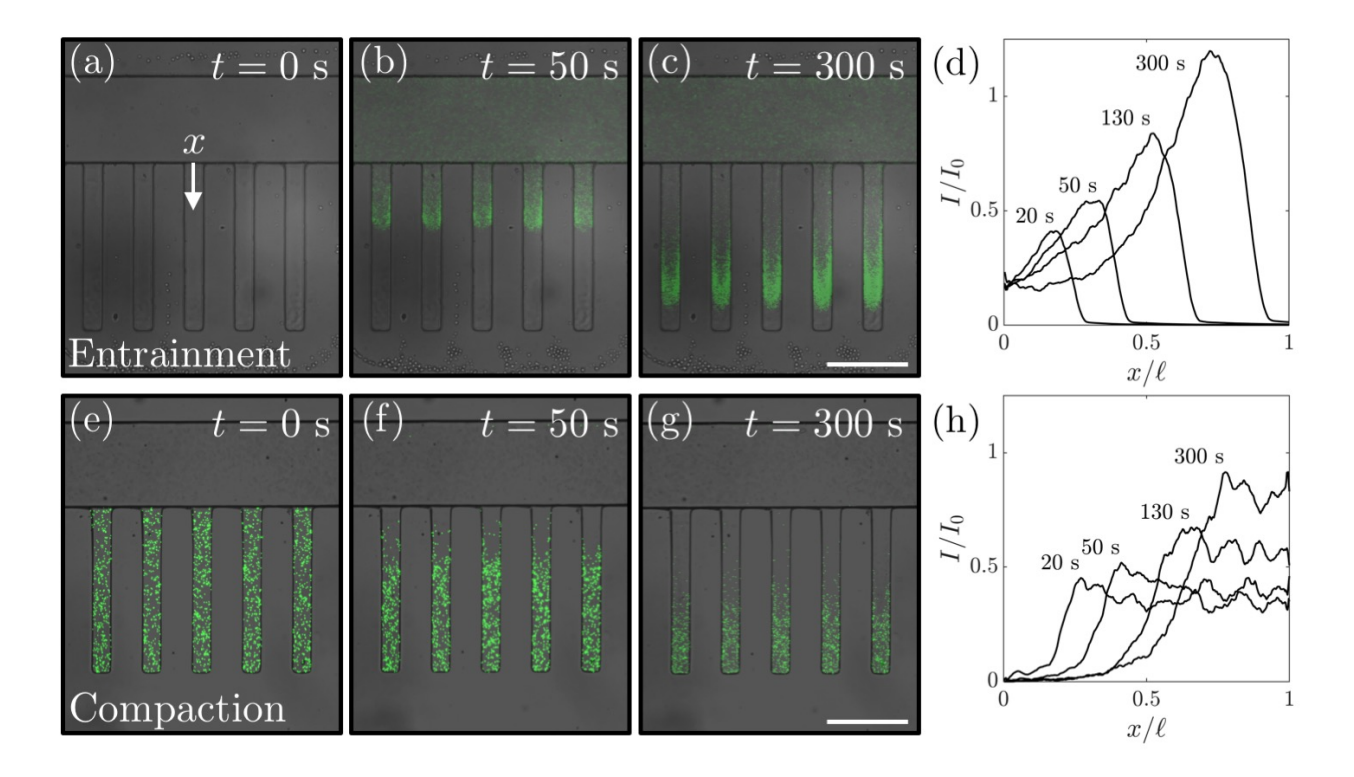


Figure 2: Time sequence of images obtained from (a-c) a typical entrainment and (e-g) a typical compaction experiment. The aggregate normalized gray value (I/I_0) of data from multiple individual experiments plotted versus length (x) along the pore (d, h), where I_0 is the initial average intensity. (a-c) The pores are initially filled with 10 mM Na₂SO₄. (e-g) The pores are initially filled with 1 μ m diameter polystyrene particles suspended in 1 mM Na₂SO₄. (a, e) At t=0 s, an air plug separates the pores from the incoming (a) particle suspension (in DI water) and (e) 0.1 mM Na₂SO₄ solution. (b-c, f-g) The diffusiophoresis of polystyrene particles is achieved in the pores. (Scale bars: 250 μ m.)

Mathematical Model

In this section, we develop a one-dimensional model to predict the diffusiophoretic motion of colloidal particles. We define x as the dimension along the length of the pore; see Fig. 2(a). We denote the ion and particle concentrations with $c_{\pm}(x,t)$ and n(x,t), respectively, where t is the time after the diffusiophoretic motion begins. We denote the valences of the ions as z_{\pm} , where $z_{+} > 0$ and $z_{-} < 0$, and the diffusion constant of ions as D_{\pm} . We denote the electrical potential as ψ and $\frac{k_{B}T}{e}$ is the thermal potential, where k_{B} is the Boltzmann constant, T is the temperature and e is the charge on an electron.

As the particle concentration is low in our experiments, we neglect the particle-particle interactions and assume that the diffusiophoretic mobility of the particles is the same as that of an isolated particle. Since the particle double layer thickness (1 - 10 nm) is much smaller than the particle size $(1 \mu\text{m})$, we also assume that the mobility of the particle is independent of its size. These conditions enable us to invoke the electroneutrality condition everywhere. Lastly, we assume that the convective flux of the ions is negligible compared with the diffusive and the electromigrative fluxes.

Based on the above assumptions, the species balance for the cations and anions is ³²

$$\frac{\partial c_{\pm}}{\partial t} = D_{\pm} \frac{\partial^2 c_{\pm}}{\partial x^2} + \frac{z_{\pm} D_{\pm}}{k_B T / e} \frac{\partial}{\partial x} \left(c_{\pm} \frac{\partial \psi}{\partial x} \right). \tag{1}$$

Equation (1) is coupled with the electroneutrality condition, or

$$z_{+}c_{+} + z_{-}c_{-} = 0. (2)$$

We can combine Equations (1) and (2) to obtain

$$\frac{\partial c_s}{\partial t} = D_a \frac{\partial^2 c_s}{\partial x^2},\tag{3}$$

where $c_s = \frac{c_+}{|z_-|} = \frac{c_-}{|z_+|}$ and D_a is the ambipolar diffusivity, which is given by

$$D_a = \frac{(z_+ - z_-)D_+D_-}{z_+D_+ - z_-D_-}. (4)$$

As is evident from Equation (4), D_a is significantly influenced by the valence of the ions. For z:z electrolytes, $D_a=\frac{2D_+D_-}{D_++D_-}$.

We can write a transport equation for the particles as

$$\frac{\partial n}{\partial t} + \frac{\partial}{\partial x} (u_p n) = D_p \frac{\partial^2 n}{\partial x^2},\tag{5}$$

where u_p is the diffusiophoretic velocity of the particles and D_p is the particle diffusivity. In electrolyte solutions, u_p is given by

$$u_p = D_{\rm DP} \frac{d\log c_s}{dx},\tag{6}$$

where $D_{\rm DP}$ is the diffusiophoretic mobility of the colloidal particles.³³

Before proceeding further, we non-dimensionalize the variables as $X = \frac{x}{\ell}$, $\tau = \frac{tD_a}{\ell^2}$, and $\Psi = \frac{\psi}{k_BT/e}$, where ℓ is the length of the pore. Equations (3) and (5) become

$$\frac{\partial c_s}{\partial \tau} = \frac{\partial c_s}{\partial X^2},\tag{7a}$$

$$\frac{\partial n}{\partial \tau} + \frac{D_{\rm DP}}{D_a} \frac{\partial}{\partial X} \left(n \frac{\partial \log c_s}{\partial X} \right) = \frac{D_p}{D_a} \frac{\partial^2 n}{\partial X^2}. \tag{7b}$$

We note that Equations (7a) - (7b) are governed by two dimensionless parameters $\frac{D_{\rm DP}}{D_a}$ and $\frac{D_p}{D_a}$. Based on our recent theoretical work on diffusiophoresis of multivalent electrolytes, ¹³ the diffusiophoretic mobility $D_{\rm DP}$ is given as

$$D_{\rm DP} = \frac{\varepsilon (k_B T/e)^2}{\mu} \left(\beta \Psi_D + \frac{1}{2} \int_0^{\Psi_D} \frac{\int_0^{\Psi_D} (z_+ \exp(-z_- \Psi') - z_+ - z_- \exp(-z_+ \Psi') + z_-)^{1/2} d\Psi'}{(z_+ \exp(-z_- \Psi_0) - z_+ - z_- \exp(-z_+ \Psi_0) + z_-)^{1/2}} d\Psi_0 \right), \tag{8}$$

where Ψ_D is the dimensionless zeta potential (i.e., the potential drop across the double layer), μ is the viscosity of the electrolyte solution, ε is the electrical permittivity of the solution, and $\beta = \frac{D_+ - D_-}{z_+ D_+ - z_- D_-}$. The term containing β is the electrophoretic contribution to diffusiophoresis and the remaining term is the chemipohoretic contribution. Both of these contributions are influenced by the choice of ion valence.

Equations (7) - (8) are solved with $c_s(X,0) = 1$, $\frac{\partial c_s}{\partial X}\big|_{X=1} = 0$, and $c_s(0,\tau) = c_0$, where c_s has been appropriately scaled. For entrainment experiments, n(X,0) = 0, $\frac{\partial n}{\partial X}\big|_{X=1} = 0$ and $n(0,\tau) = 1$, where n has been appropriately scaled. For compaction experiments, n(X,0) = 1, $\frac{\partial n}{\partial X}\big|_{X=1} = 0$ and $n(0,\tau) = 0$. The numerical solution procedure and parameter values are discussed below in the Computational Method subsection. We tabulate the values

of D_a and $D_{\rm DP}$ for the electrolytes used in our study in Table 2.

Table 2: This work examines six ubiquitous electrolytes with a variety of valences. The $D_{\rm a}$ values were calculated from Equation (4) and $D_{\rm DP}$ values were calculated from Equation (8). The ion diffusivity values were obtained from Velegol et al.³³

Salt	$D_+ \times 10^{-9} [m^2/s]$	$D_{-} \times 10^{-9} [m^2/s]$	$D_{\rm a} \times 10^{-9} [m^2/s]$	$D_{\rm DP} \times 10^{-9} [m^2/s]$	$\frac{\mathrm{D_{DP}}}{\mathrm{D_{a}}}$
NaCl	1.33	2.03	1.6	0.73	0.46
Na_2SO_4	1.33	1.07	1.2	0.37	0.31
$CaCl_2$	0.793	2.03	1.3	0.49	0.38
$CaSO_4$	0.793	1.07	0.90	0.26	0.29
MgCl_2	0.705	2.03	1.2	0.53	0.44
$MgSO_4$	0.705	1.07	0.85	0.28	0.33

Computational Method

Equation (7a) can be solved analytically to obtain a series solution, given as

$$c_s(X,\tau) = c_0 + (1 - c_0) \sum_{k=0}^{\infty} \frac{2}{\lambda_k} \sin(\lambda_k X) \exp\left(-\lambda_k^2 \tau\right), \tag{9}$$

where $\lambda_k = (2k+1)\frac{\pi}{2}$. This solution is used to numerically evaluate $\frac{\partial \log c_s}{\partial X}$. Finally, we numerically integrate Equation (7b) using the method of lines to evaluate $n(X,\tau)$. The values of the physical parameters used are $\ell = 500~\mu\text{m}$, $\mu = 10^{-3}~\text{Pa·s}$, $\varepsilon = 7 \times 10^{-10}~\text{F/m}$, $D_p = 2 \times 10^{-13}~\text{m}^2/\text{s}$, and $k_BT/e = 25~\text{mV}$ (assuming T = 298~K). In entrainment experiments, DI water is used in the main channel, or $c_0 = 0$ (Table 1). However, due to the singularity in evaluating $\frac{\partial \log c_s}{\partial x}$ at c_0 , we set $c_0 = 10^{-3}$ to model entrainment experiments. We choose a sufficiently small c_0 to ensure that X_{peak} is independent of c_0 (see Supporting Information). $c_0 = 0.1$ is used to model compaction experiments (see Table 1). The values of D_+ and D_- are provided in Table 2. A value of $\Psi_D = -2$ is used for calcium and magnesium salts, whereas $\Psi_D = -3$ is used for sodium salts. ³⁴

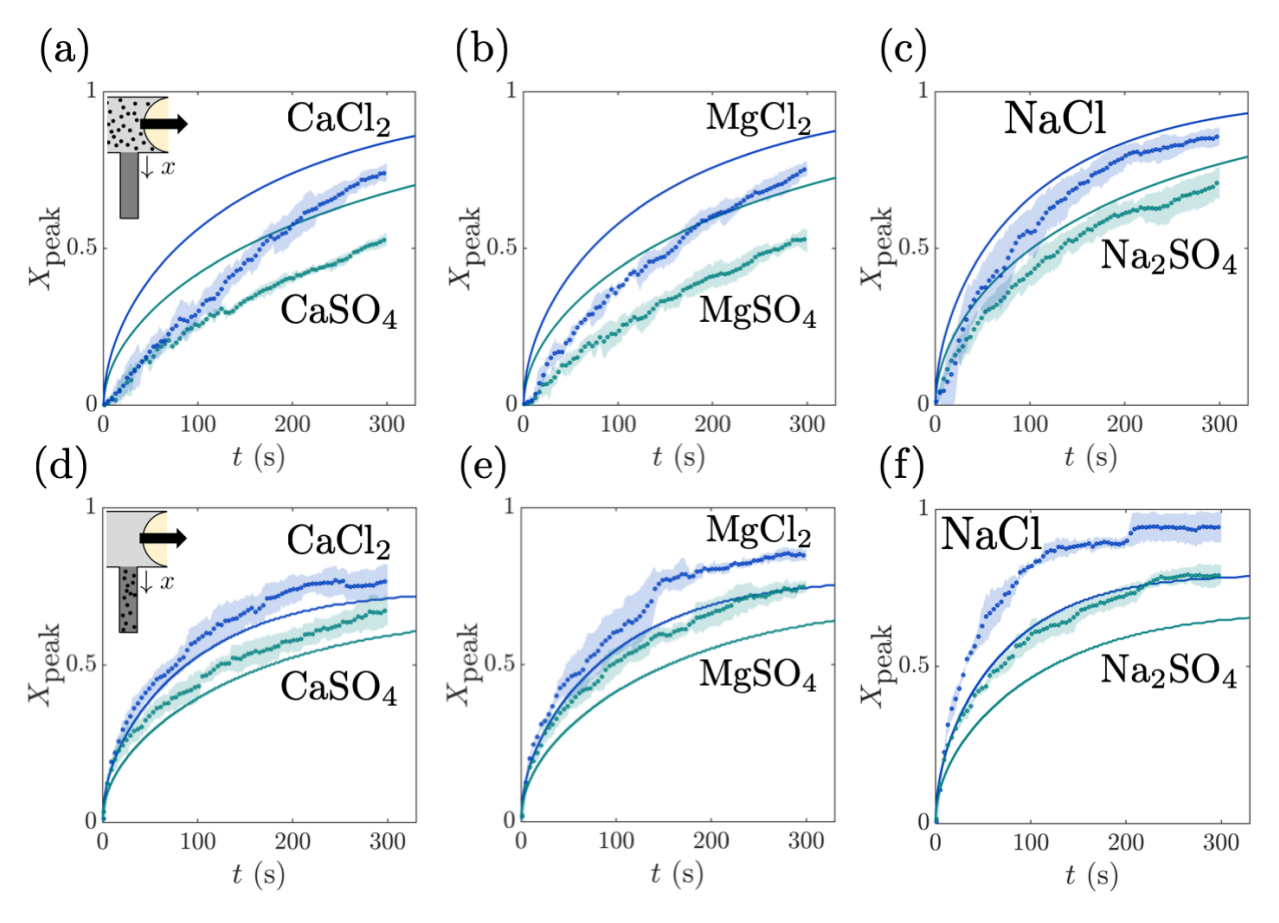


Figure 3: The peaks identified from the experimental time series data were plotted as a function of time and compared with predictions from theory. The shaded region represents the standard deviation. The model (Equation (7b), represented by solid lines) is an overestimate of the peak position achieved by the particles in the entrainment experiments (a-c), and an underestimate for the compaction experiments (d-f). In all cases, the chloride salts travel further than the sulfate salts in the same time interval. Note that every fourth experimental point was plotted for clarity.

Discussion

To understand the influence of electrolyte valence on the diffusiophoretic motion of the particles, we define $X_{\text{peak}}(t) = \frac{x_{\text{peak}}}{\ell}$ as the location of the global maximum in an intensity plot (see Figs. 2(d), 2(h)). Similarly, we obtain $X_{\text{peak}}(t)$ from the mathematical model by numerically evaluating the location of the maximum in $n(X,\tau)$. We report $X_{\text{peak}}(t)$ for the six different electrolytes and for both entrainment and compaction experiments in Fig. 3.

We observe that the diffusiophoretic movement of particles in the presence of sulfate salts,

i.e., CaSO₄, MgSO₄ and Na₂SO₄, is slower than in the presence of the corresponding chloride salts, i.e., CaCl₂, MgCl₂ and NaCl. This is observed in both entrainment (Fig. 3(a-c)) and compaction experiments (Fig. 3(d-f)). We find that our model is in qualitative agreement with experimental data and is able to capture the differences between sulfate and chloride salts without any fitting parameters.

We seek to understand the physics that gives rise to a slower diffusiophoretic movement in sulfate salts as compared to chloride salts. Firstly, we note that since $\frac{D_p}{D_{\mathrm{DP}}} = \mathcal{O}(10^{-3})$, particle diffusivity has a negligible effect on the motion of the particles. To determine the value of X_{peak} without numerically solving Equations (7)-(8), we assume that the channel is semi-infinite, or $0 \leq X \leq \infty$. We introduce a similarity variable of the form $\eta = \frac{X}{\sqrt{4\tau}}$ to transform Equations (7a) and (7b) as

$$2\eta \frac{dC_s}{d\eta} + \frac{d^2C_s}{d\eta^2} = 0, (10a)$$

$$\left(2\eta - \frac{D_{\rm DP}}{D_a} \frac{d\log C_s}{d\eta}\right) \frac{dN}{d\eta} - \frac{D_{\rm DP}}{D_a} N \frac{d^2 \log C_s}{d\eta^2} + \frac{D_p}{D_a} \frac{d^2 N}{d\eta^2} = 0, \tag{10b}$$

where $C_s(\eta) = c_s(X, \tau)$ and $N(\eta) = n(X, \tau)$. Equation (10a) is subjected to boundary conditions $C_s(0) = c_0$ and $C_s(\infty) = 1$, and thus yields the solution

$$C_s(\eta) = c_0 + (1 - c_0)\operatorname{erf}(\eta),$$
 (11)

where $\operatorname{erf}(\eta)$ is the error function. Equation (10b) is subject to boundary conditions N(0) = 1 and $N(\infty) = 0$ for the entrainment scenario, and N(0) = 0 and $N(\infty) = 1$ for the compaction scenario. Using the result from Eq. (11), we numerically solve Equation (10b) by using the finite-difference method.

The dependence of $N(\eta)$ for the entrainment scenario and different values of $\frac{D_{\text{DP}}}{D_a}$ is provided in Fig. 4(a). We observe that η_{peak} , i.e., the η where N is maximum, increases with increasing $\frac{D_{\text{DP}}}{D_a}$. This trend implies that an increase in diffusiophoretic mobility leads

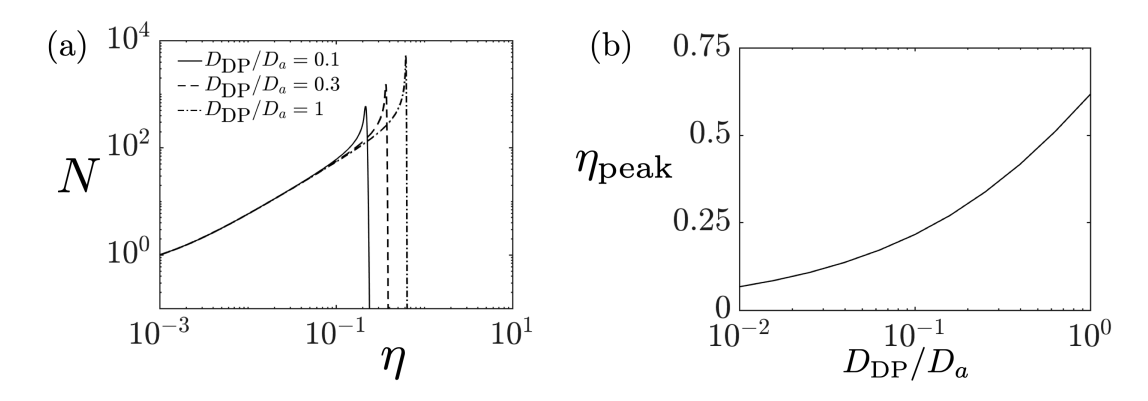


Figure 4: Overview of the predictions of Equation (10b). (a) $N(\eta)$ for different $\frac{D_{\rm DP}}{D_a}$. We define $\eta_{\rm peak}$ as the location where $N(\eta)$ is maximum. (b) Variation of the $\eta_{\rm peak}$ for different $\frac{D_{\rm DP}}{D_a}$. The results were calculated for fixed values of $\frac{D_p}{D_a} = 10^{-4}$ and $c_0 = 10^{-3}$.

to deeper penetration of particles. The dependence of $\eta_{\rm peak}$ on $\frac{D_{\rm DP}}{D_a}$ is presented in Fig. 4(b).

We emphasize that η_{peak} is a function of $\frac{D_{\text{DP}}}{D_a}$ and thus changes for different electrolytes. We plot $2\eta_{\text{peak}}\sqrt{\tau}$ against X_{peak} (recall that $\eta = \frac{X}{\sqrt{4\tau}}$); see Fig. 5. We observe reasonable collapse of the theoretical results (Equation (7b), Fig. 5(a)) as well as of the experimental results (see Fig. 5(b)) for all of the different electrolytes. We acknowledge that the collapse of the experimental data is qualitative. However, it does enable us to highlight the relative importance of the diffusiophoretic mobility and the ambipolar diffusivity.

For the electrolytes used in our study, i.e., NaCl, Na₂SO₄, CaCl₂, CaSO₄, MgCl₂ and MgSO₄, $\frac{D_{\rm DP}}{D_a}$ varies between 0.28 and 0.45. Therefore, $\eta_{\rm peak}$ is roughly constant for the different electrolytes (see Fig. 4(b)) and the diffusiophoretic motion is dominated by $\tau = \frac{D_a t}{\ell^2}$. Physically, D_a dictates the timescale at which the concentration gradient of electrolyte evolves, which in turn sets the diffusiophoretic motion. We highlight that cation and anion valences influence D_a (see Equation (4)), and thus ion valences can be exploited to tune the diffusiophoretic motion of the particles.

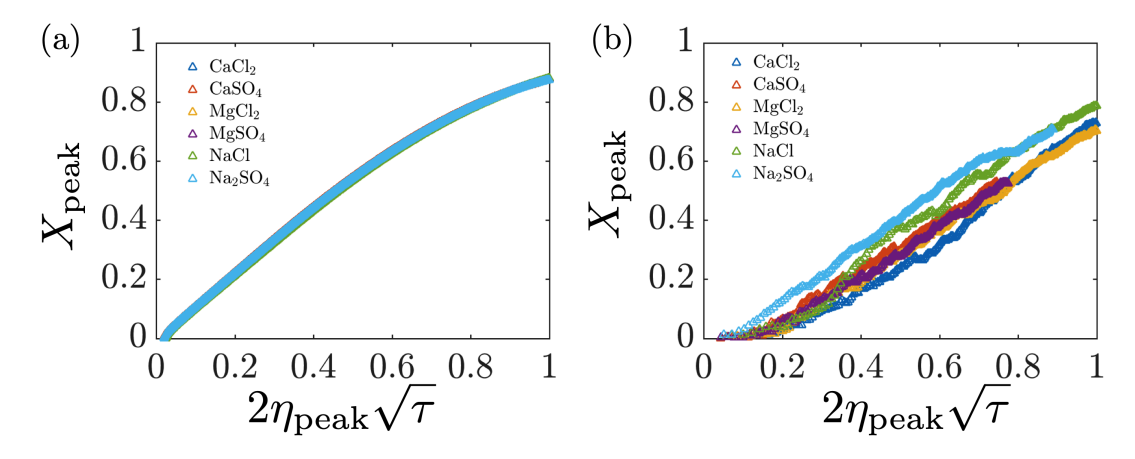


Figure 5: Collapse of X_{peak} versus $2\eta_{\text{peak}}\sqrt{\tau}$ for different electrolytes for (a) the model (Equation (7b)) and (b) the experimental data; $\tau = \frac{tD_a}{\ell^2}$. The data presented here is obtained from the entrainment experiments.

Conclusions

In conclusion, we investigated the diffusiophoretic motion of 1 μ m diameter polystyrene particles in six different electrolytes with different cation and anion valences. We observed that chloride salts lead to faster diffusiophoretic motion than the sulfate salts for both entrainment and compaction experiments. We developed a mathematical model that is able to predict the behavior of the distribution of the colloidal particles without any fitting parameters.

Our analysis highlights that the ambipolar diffusivity, which is a function of ion diffusivities and valences, dominates the time scale of diffusiophoretic motion. Therefore, ion valence can be exploited to tune the diffusiophoretic focusing of particles, ^{7,14} manipulate the motion of active colloidal particles, ²⁷ and measure the zeta-potential of charged species, ³⁴ among other applications. Our results will motivate future fundamental research of diffusiophoresis, and more broadly electrokinetics, ^{35,36} with mixtures of multivalent electrolytes.

Associated Content

Supporting Information – Discussion of difficulties working at high concentration, demonstration of the nearly-constant intensity of compaction experiments, data analysis for Figure 3, discussion of the effect of the concentration ratio on diffusiophoretic motion of particles, and videos.

Acknowledgements

We gratefully acknowledge Professor Robert Prud'homme, and Dr. Navid Bizmark (Department of Chemical and Biological Engineering, Princeton University) for insightful discussions. This work was financially supported by the National Science Foundation (CBET-1702693). S.S. and H.A.S. directed the experimental research and A.G. and H.A.S. directed the modeling. S.S. and J.L.W. designed the experiments. J.L.W. performed the experiments. Y.E.Y. and J.L.W. performed the image processing and data analysis. A.G. performed the modeling and developed the model. A.G., S.S., H.A.S., and J.L.W. wrote the manuscript.

References

- (1) Derjaguin, B.; Sidorenkov, G.; Zubashchenkov, E.; Kiseleva, E. Kinetic phenomena in boundary films of liquids. *Kolloidn. Zh* **1947**, *9*, 335–347.
- (2) Prieve, D.; Anderson, J.; Ebel, J.; Lowell, M. Motion of a particle generated by chemical gradients. Part 2. Electrolytes. *Journal of Fluid Mechanics* **1984**, *148*, 247–269.
- (3) Prieve, D. C.; Roman, R. Diffusiophoresis of a rigid sphere through a viscous electrolyte solution. *Journal of the Chemical Society, Faraday Transactions 2: Molecular and Chemical Physics* **1987**, *83*, 1287–1306.

- (4) Keh, H. J.; Ma, H. C. Diffusioosmosis of electrolyte solutions along a charged plane wall. *Langmuir* **2005**, *21*, 5461–5467.
- (5) Staffeld, P. O.; Quinn, J. A. Diffusion-induced banding of colloid particles via diffusiophoresis: 1. Electrolytes. *Journal of Colloid and Interface Science* **1989**, *130*, 69–87.
- (6) Ebel, J.; Anderson, J. L.; Prieve, D. Diffusiophoresis of latex particles in electrolyte gradients. *Langmuir* **1988**, *4*, 396–406.
- (7) Abécassis, B.; Cottin-Bizonne, C.; Ybert, C.; Ajdari, A.; Bocquet, L. Boosting migration of large particles by solute contrasts. *Nature Materials* **2008**, *7*, 785.
- (8) Kar, A.; Chiang, T.-Y.; Ortiz Rivera, I.; Sen, A.; Velegol, D. Enhanced transport into and out of dead-end pores. *ACS Nano* **2015**, *9*, 746–753.
- (9) Banerjee, A.; Williams, I.; Azevedo, R. N.; Helgeson, M. E.; Squires, T. M. Soluto-inertial phenomena: Designing long-range, long-lasting, surface-specific interactions in suspensions. *Proceedings of the National Academy of Sciences* 2016, 113, 8612–8617.
- (10) Banerjee, A.; Squires, T. M. Long-range, selective, on-demand suspension interactions: Combining and triggering soluto-inertial beacons. *Science Advances* **2019**, *5*, eaax1893.
- (11) Palacci, J.; Cottin-Bizonne, C.; Ybert, C.; Bocquet, L. Osmotic traps for colloids and macromolecules based on logarithmic sensing in salt taxis. Soft Matter 2012, 8, 980– 994.
- (12) Shin, S.; Warren, P. B.; Stone, H. A. Cleaning by surfactant gradients: Particulate removal from porous materials and the significance of rinsing in laundry detergency. *Physical Review Applied* **2018**, *9*, 034012.
- (13) Gupta, A.; Rallabandi, B.; Stone, H. A. Diffusiophoretic and diffusioosmotic velocities for mixtures of valence-asymmetric electrolytes. *Physical Review Fluids* 2019, 4, 043702.

- (14) Shi, N.; Nery-Azevedo, R.; Abdel-Fattah, A. I.; Squires, T. M. Diffusiophoretic focusing of suspended colloids. *Physical Review Letters* **2016**, *117*, 258001.
- (15) Shin, S.; Um, E.; Sabass, B.; Ault, J. T.; Rahimi, M.; Warren, P. B.; Stone, H. A. Size-dependent control of colloid transport via solute gradients in dead-end channels.

 *Proceedings of the National Academy of Sciences 2016, 113, 257–261.
- (16) Ault, J. T.; Shin, S.; Stone, H. A. Diffusiophoresis in narrow channel flows. *Journal of Fluid Mechanics* **2018**, *854*, 420–448.
- (17) Battat, S.; Ault, J. T.; Shin, S.; Khodaparast, S.; Stone, H. A. Particle entrainment in dead-end pores by diffusiophoresis. *Soft Matter* **2019**, *15*, 3879–3885.
- (18) Nery-Azevedo, R.; Banerjee, A.; Squires, T. M. Diffusiophoresis in ionic surfactant gradients. *Langmuir* **2017**, *33*, 9694–9702.
- (19) Shin, S.; Shardt, O.; Warren, P. B.; Stone, H. A. Membraneless water filtration using CO₂. Nature Communications **2017**, 8, 15181.
- (20) Florea, D.; Musa, S.; Huyghe, J. M.; Wyss, H. M. Long-range repulsion of colloids driven by ion exchange and diffusiophoresis. *Proceedings of the National Academy of Sciences* 2014, 111, 6554–6559.
- (21) Prieve, D. C.; Malone, S. M.; Khair, A. S.; Stout, R. F.; Kanj, M. Y. Diffusiophoresis of charged colloidal particles in the limit of very high salinity. *Proceedings of the National Academy of Sciences* 2018, 201701391.
- (22) Warren, P. B.; Shin, S.; Stone, H. A. Diffusiophoresis in ionic surfactants: effect of micelle formation. *Soft Matter* **2019**, *15*, 278–288.
- (23) Ault, J. T.; Warren, P. B.; Shin, S.; Stone, H. A. Diffusiophoresis in one-dimensional solute gradients. *Soft Matter* **2017**, *13*, 9015–9023.

- (24) Khair, A. S. Diffusiophoresis of colloidal particles in neutral solute gradients at finite Péclet number. *Journal of Fluid Mechanics* **2013**, 731, 64–94.
- (25) Frankel, A. E.; Khair, A. S. Dynamics of a self-diffusiophoretic particle in shear flow. *Physical Review E* **2014**, *90*, 013030.
- (26) Chiang, T.-Y.; Velegol, D. Multi-ion diffusiophoresis. *Journal of Colloid and Interface Science* **2014**, 424, 120–123.
- (27) Aubret, A.; Youssef, M.; Sacanna, S.; Palacci, J. Targeted assembly and synchronization of self-spinning microgears. *Nature Physics* **2018**, *14*, 1114.
- (28) Prieve, D. C. Migration of a colloidal particle in a gradient of electrolyte concentration.

 Advances in Colloid and Interface Science 1982, 16, 321–335.
- (29) Lin, M. M.-J.; Prieve, D. C. Electromigration of latex induced by a salt gradient.

 Journal of Colloid and Interface Science 1983, 95, 327–339.
- (30) Hartman, S. V.; Božič, B.; Derganc, J. Migration of blood cells and phospholipid vesicles induced by concentration gradients in microcavities. *New Biotechnology* **2018**, *47*, 60–66.
- (31) Wirsching, F. Calcium sulfate. Ullmann's Encyclopedia of Industrial Chemistry 2000,
- (32) Deen, W. M. Analysis of Transport Phenomena; Oxford University Press, New York, 2012.
- (33) Velegol, D.; Garg, A.; Guha, R.; Kar, A.; Kumar, M. Origins of concentration gradients for diffusiophoresis. *Soft Matter* **2016**, *12*, 4686–4703.
- (34) Shin, S.; Ault, J. T.; Feng, J.; Warren, P. B.; Stone, H. A. Low-cost zeta potentiometry using solute gradients. *Advanced Materials* **2017**, *29*.

- (35) Gupta, A.; Stone, H. A. Electrical double layers: effect of asymmetry in electrolyte valence on steric effects, dielectric decrement and ion-ion correlations. *Langmuir* **2018**, 34, 11971–11985.
- (36) Bazant, M. Z.; Thornton, K.; Ajdari, A. Diffuse-charge dynamics in electrochemical systems. *Physical Review E* **2004**, *70*, 021506.

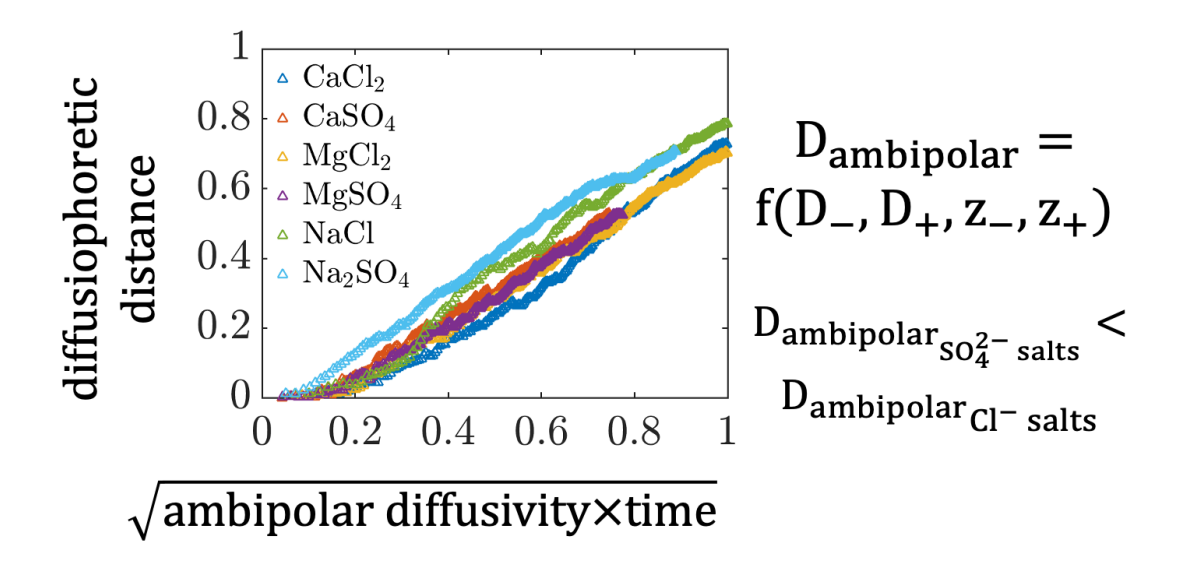


Figure 6: For Table of Contents Only